Article

An Experimental Investigation on the Shear-Seepage Coupling Failure Behavior of Split Grouting-Reinforced Body

Yaolei Zhang [1], **Haitong Sui** [1,2,*], **Lei Yang** [1] **and Rongfeng Lin** [1]

1   Geotechnical and Structural Engineering Research Center, Shandong University, Jinan 250061, China;
     m17865199868@163.com (Y.Z.); yanglei@sdu.edu.cn (L.Y.); lin201057@163.com (R.L.)
2   Institute of Urban Innovation, Yokohama National University, Yokohama 2408501, Japan
*   Correspondence: haitongsui@gmail.com; Tel.: +86-18563725637

Abstract: A split grouting-reinforced body (SGRB) is the new surrounding rock that forms after split grouting reinforcement in tunnels and underground engineering, and its shear-seepage behavior is one of the critical factors affecting tunnel stability. The effects of seepage pressure, confining pressure, and the roughness of the soil–slurry interface on the shear-seepage characteristics of SGRB specimens were investigated using a modified triaxial shear-seepage coupling test system. The failure mechanism for the SGRB was analyzed taking into account its seepage behavior and mechanical characteristics. The results showed that the seepage process of the SGRB specimens could be divided into four stages according to the seepage velocity, including the waterless, rapid, decelerating, and steady seepage stages, and the corresponding water turbidity in the seepage stages was classified as turbid, mildly turbid, or clear, respectively. The peak shear stress of the soil–slurry interface of the SGRB specimens under seepage was lower than that in the waterless environment, and the peak shear stress decreased from 57.25 kPa (waterless) to 29.37 kPa (a seepage pressure of 0.08 MPa), marking a reduction of 50.74%. The seepage phenomenon of the specimens was related to the 'seepage-to-confining ratio', and its critical points in the waterless, seepage, and seepage surge stages were 0.2, 0.4, and 0.6, respectively.

Keywords: split grouting-reinforced body; soil–slurry interface; seepage pressure; confining pressure; failure mechanism

1. Introduction

Grouting technology is an effective method used to reinforce water-rich soft strata and can improve the stability of surrounding rocks and ensure safety during tunnel construction [1–5]. The soft surrounding rock is split and compacted with cement grouting under injection pressure [6–10], forming a split grouting-reinforced body (SGRB) [11]. However, it should be noted that SGRBs exist in complex geological environments [12]. Under the coupling effect of geo-stress and groundwater, the SGRB will undergo deformation. Due to differences in their mechanical properties, the deformation of slurry veins and soft rocks is inconsistent. This disparity leads to shear failure at the interface between the soil and slurry veins (soil–slurry interface), forming a seepage path. The performance of the SGRB is one of the key factors affecting the stability of the surrounding rocks. Therefore, investigating the shear-seepage coupling failure behavior of SGRBs is crucial for predicting the stability of the surrounding rocks.

Recently, researchers have attached importance to research on the physical and mechanical properties of grouting-reinforced bodies, achieving certain results [13–15]. Liu et al. [16] investigated the mechanical properties of a sand-filled GRB under different seepage pressures. Yin et al. [17] studied the creep behavior of sand-filled GRBs under different loadings. The law of mechanical property degradation of sand GRBs under seawater erosion was studied, and a constitutive model was established [18]. Huang et al. [19] analyzed the influence of the water content of argillaceous siltstone on the strength of filled

GRBs. Zang et al. [20] investigated the influence of broken coal with different particle sizes on the bearing capacity of broken-coal-filled GRBs. Peng et al. [21] proposed a new method of predicting the mechanical properties of filled GRBs considering the porosity and the cement-grouting filling rate. Taking fractured red sandstone GRBs as research objects, a series of shear tests were carried out to study the relationship between the shear strength of the filled GRBs and the shear angle [22]. Previous studies have focused on the performance of filled GRB specimens, but little attention has been paid to the mechanical properties and seepage characteristics of SGRBs.

It is noteworthy that the soil–slurry interface is a weak area of SGRBs [23]. However, many researchers have focused on studying the performance of interfaces between soil and various structures, including concrete, pile, steel, geogrid-reinforced steel slags, and others, via direct shear tests [24–29]. The microscopic deformation mechanism of the shear zone between a pre-bored, grouted, planted nodular pile and warm frozen ground was investigated [25]. Peng et al. [30] investigated the mechanical behavior of the interface between coarse-grained soil and concrete and analyzed the effects of mixed soil slurry on the mechanical properties of the interface. At present, regarding the soil–slurry interface in SGRBs, there are developments that require further elaboration in terms of mechanical performance and seepage behavior.

The shear-seepage characteristics of the soil–slurry interface represent one of the factors determining the mechanical properties of an SGRB. Previously, researchers have modified traditional direct shear instruments to study the shear-seepage behavior of joint rock masses [31–33]. However, most studies on the shear stress of soil–slurry interfaces used direct shear tests [23,28,34,35]. Due to SGRBs' complex geological environments, studying the shear performance of the soil–slurry interface requires one to consider the confining pressure and seepage pressure.

In this study, a shear-seepage coupling test system was designed in a triaxial stress environment, considering the typical structure of the soil–slurry interface in the GRB. The failure behavior, mechanical characteristics, and seepage characteristics of the SGRB in completely weathered granite under triaxial shear-seepage were experimentally investigated. The triaxial shear-seepage tests were carried out, and the effects of seepage pressure, confining pressure, and soil–slurry interface roughness on the peak shear stress and the seepage characteristics were determined. The effects of confining pressure and seepage pressure on the water turbidity, seepage velocity, and seepage quality of the GRB are discussed.

2. Experimental Outline

2.1. Modified Triaxial Shear-Seepage Coupling Test System

Figure 1 shows the modified triaxial shear-seepage test system based on the original triaxial test system. The modified principle of the test system is shown in Figure 1a, where additional pads are placed at both ends of the specimen. Specifically, the lower surface of the upper pad is only in contact with the slurry vein and the area is equal, and the lower pad is in contact with the soil and the area is equal. In this way, the axial stress applied to the specimen is changed to direct shear stress, and the direct shear displacement is reserved. Simultaneously, the upper pad is designed with holes for water flow-through. In this way, the original seepage flow path through the specimen is preserved, and the slurry vein can undergo axial displacement. Moreover, a layer of plastic roll material is added between the specimen and the rubber mold, so that the seepage water in the upper pad is not affected by the confining pressure. Vaseline is applied to the plastic to prevent water from flowing into the gap between the plastic and the specimen. In order to prevent the pads from moving inward under the confining pressure, the length of the slurry vein at the lower end of the specimen exceeds the soil. The GRB specimens containing the soil–slurry interface can be in an environment where direct shear stress, seepage pressure, and confining pressure are applied simultaneously under the above improvements. Accordingly, this modified test system is suitable for testing the shear-seepage coupling performance of SGRB specimens.
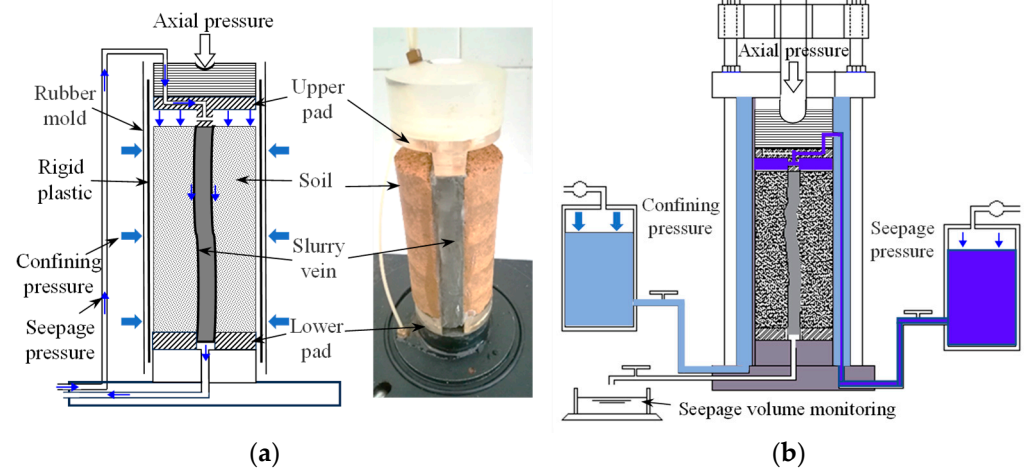
Figure 1. Apparatus of triaxial shear-seepage coupling tests. (**a**) Triaxial pressure chamber and specimen diagram. (**b**) Triaxial shear-seepage coupling test system.

Figure 1b shows the modified experimental system, which can be used to monitor the seepage water quality and water turbidity in real time. The variations in seepage water quality and water turbidity can reflect the shear-seepage failure behavior of the GRB. The performance of the modified experimental system is represented in Table 1. The test conditions include a shear rate of 0.8 mm/min and a maximum test shear displacement of 8 mm.

Table 1. Performance indicators of the modified experimental system.

Performance Indicators	Maximum Value	Accuracy
Shear force	3 kN	1 N
Shear displacement	8 mm	0.08
Shear displacement loading rate	2.4 mm/min	-
Confining pressure	3 MPa	0.1 MPa
Seepage pressure	1 MPa	0.01 MPa

2.2. SGRB Specimens Containing a Soil–Slurry Interface

The SGRB is a composite of slurry veins and soil formed under the intrusion of cement grouting into the soil via a compression-splitting action. Accordingly, the GRB specimens used in this study contained slurry veins. The structural form and fabrication of the GRBs are shown in Figure 2. The elongated slurry vein is wrapped in two semi-cylindrical soils to form a cylindrical GRB specimen. The interfaces between the soil and the slurry veins (the soil–slurry interface) match the characteristics of a standard joint roughness curve (JRC) [36]. The steps for producing the GRB specimens were as follows: Firstly, taking completely weathered granite from the tunnel site treated with grouting reinforcement as the spoil, the cylindrical soil was prepared using the standard remodeling method, and the remodeling index was the density of the completely weathered granite after grouting reinforcement. The cylindrical soil was then divided into two half-cylinders with a linear saw. The cut surface of the half-cylinder soil body was polished with a plane, and the polished cut surface conformed to the JRC characteristics. Then, the slurry veins were filled with standard ordinary cement (P.O. 42.5) in pouring molds with the characteristics of the JRC. The filled slurry veins were maintained for 7 days according to the standard procedure. Finally, the two half-cylinders and the slurry were bonded with cement grouting to form a cylindrical GRB specimen and were used for testing after 24 h. The water–cement ratio of the cement grouting was 0.8, and the size of the GRB specimen was 61.8 × 125 mm (diameter × height).
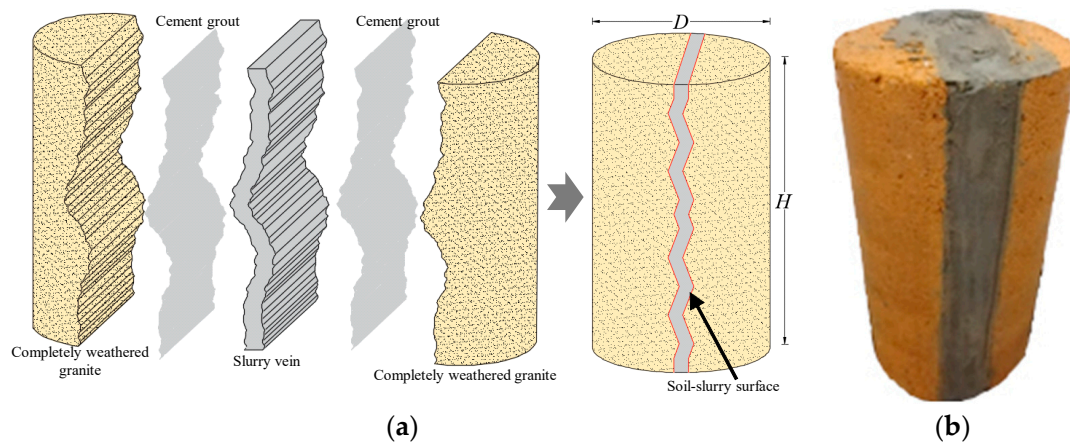
Figure 2. Specimen fabrication method. (**a**) Composition of the specimen. (**b**) Nature of specimen with a JRC of 0–2.

2.3. Experimental Conditions

The experimental conditions were designed for three series of tests based on different confining pressures, seepage pressures, and JRCs, respectively, as shown in Table 2. The confining pressure and seepage pressure were the environment conditions of the specimen in the triaxial shear-seepage test. The JRC was the characteristic of the soil–slurry interface when the specimen was fabricated.

Table 2. Triaxial shear and seepage conditions of the laboratory test.

Specimen No.	Confining Pressure (MPa)	Seepage Pressure (MPa)	JRC
S-1, 2, 3, 4, 5	0.1	0, 0.02, 0.04, 0.06, 0.08	4–6
J-1, 2, 3, 4, 5	0.1	0.08	0–2, 4–6, 8–10, 12–14, 16–18
C-1, 2, 3, 4, 5	0.1, 0.2, 0.4, 0.6, 0.8	0.08	4–6

3. Analysis of the Shear-Seepage Coupling Failure Characteristics of SGRB

The failure behavior of the SGRB specimens was analyzed by observing the variations in shear stress, seepage velocity, and water turbidity with shear displacement during the shear-seepage coupling process.

3.1. Performance of Failure Behavior

Figure 3 shows the variations in shear stress and seepage velocity with shear displacement in the shear-seepage coupling tests of the GRB, illustrating test results derived under two sets of test conditions. One refers to the general conditions in the series of tests: the confining pressure, seepage pressure, and JRC are 0.1 MPa, 0.08 MPa, and 4–6, respectively. The corresponding shear stresses under these test conditions are shown as green square lines in the figure, and the seepage rates are shown as blue triangles and fitted with quadratic functions. The other is a seepage pressure of 0 MPa, with the same confining pressure and JRC as the above test conditions. The test results for these test conditions are shown with the shear stress curve alone, indicated with the line of black circles.
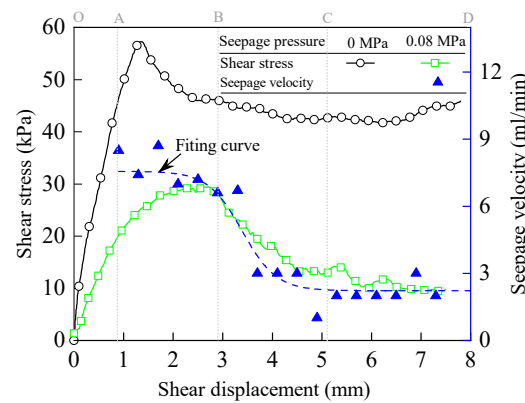
Figure 3. Variations in shear stress and seepage velocity with the shear displacement of the GRB.

The variation in seepage velocity with shear displacement has obvious stage characteristics. The shear-seepage process of the GRB specimens can be partitioned into four distinct stages: a waterless stage, a rapid seepage stage, a decelerating seepage stage, and a steady seepage stage. These four stages correspond to the OA, AB, BC, and CD sections in the figure. In stage OA, the shear stress increased almost linearly with the increasing shear displacement. No seepage of water through the GRB specimen was observed. In stage AB, the shear stress gradually increased to reach its peak, and the shear modulus gradually decreased. The seepage velocity suddenly increased to a maximum value of 7.5 mL/s and then gradually decreased. In stage BC, the shear stress and shear velocity decreased. In stage CD, the shear stress and seepage velocity gradually stabilized to 9.7 kPa and 2.2 mL/s, respectively.

3.2. Mechanical Characteristics of the SGRB Specimens

The mechanical characteristics of the SGRB specimens were influenced by the presence of seepage water. As shown in Figure 3, the shear-stress–displacement curve demonstrates a shear hardening behavior in the waterless environment. The shear stress increases to a peak stress of 57.25 kPa and then decreases to a residual stress of 41.87 kPa with displacement. However, the mechanical properties of the soil–slurry interface within the SGRB are altered in the presence of groundwater. Under seepage conditions, the shear-stress–displacement curve exhibits shear softening. The shear stress increases with displacement until it reaches a peak shear stress of 29.37 kPa. Then, the shear stress gradually decreases, settling at a residual stress of 10.10 kPa when subjected to a seepage pressure of 0.08 MPa. These test results unequivocally illustrate that seepage water leads to the softening of the soil–slurry interface. This softening effect can be attributed to the reduction in the level of cohesion between soil particles caused by the seepage water.

In the waterless environment, the raised slurry veins within the soil–slurry interface of the GRB cut through the soil and form a shear surface under shear action. After the peak shear stress, the shear stress is converted from static friction to dynamic friction and presented as residual shear stress. In the seepage environment, water invades the shear surface and gradually softens the soil. The seepage water reduces the cohesion and internal friction angle of the soil and both sides of the shear surface, thereby causing a reduction in shear strength. The water increases the shear area so that more soils are sheared, which causes the peak shear displacement to increase. After the peak shear stress, the water dissolves the soil micro-particles to form a soil slurry. The soil slurry fills and lubricates the shear surface and reduces its friction coefficient, thereby making the residual shear stress smaller.

3.3. Seepage Characteristics of the SGRB Specimens

The variation in seepage velocity with shear displacement demonstrates distinct phases, which correspond with the stages of water turbidity observed during seepage.

These water turbidity stages are classified as turbid, mildly turbid, and clear, as shown in Figure 4. These three stages correspond to the AB, BC, and CD stages of seepage velocity, respectively.
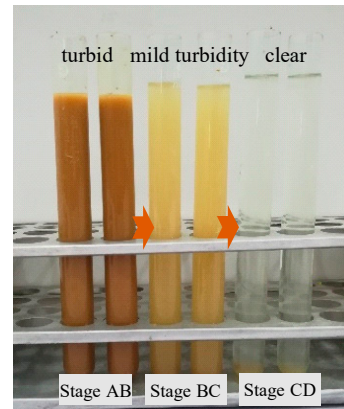

Figure 4. Turbidity of seepage water.

During stage AB, the seepage water permeates the soil–slurry interface, causing the transport of soil particles around the soil–slurry interface with seepage water, forming the seepage channels, and the turbid water flows from the channels, as shown in Figure 4 for the AB stage. Under the confining pressure, a new contact surface is formed between the slurry veins and the soil. The seepage water through the shear surface of the seepage path gradually tends to become curved. Therefore, the seepage velocity gradually decreases. In stage BC, the seepage path coincides with the undulation of the soil–slurry interface. The seepage water softens the shear surface and acts as a filter. Therefore, the seepage velocity decreases rapidly, and the soil content in the seepage decreases. This leads the water to attain a state of mild turbidity, as shown in Figure 4 for the BC stage. In stage CD, the softened soil fills the seepage path, causing a change from seepage to infiltration at the shear surface. Consequently, the seepage velocity tends to stabilize, and the outflow water becomes clear, as shown in Figure 4 for the CD stage.

4. Analysis of the Shear-Seepage Characteristics of the SGRB

The GRB has a complex geological environment, and its performance is affected by groundwater, geo-stress, and other factors. Therefore, it is necessary to further investigate the influences of the seepage pressure, confining pressure, and roughness of the soil–slurry interface on the peak shear stress, peak shear displacement, and seepage phenomenon based on the above analysis of the shear-seepage behavior of the GRB. In this section, the laws of different factors influencing the mechanical properties and seepage behavior of the GRB are analyzed, and the failure mechanism of the GRB is summarized.

4.1. Analysis of Seepage Pressure Effects on the Properties of Splitting GRB Specimens

Seepage pressure is an important factor accelerating the deterioration of the mechanical properties of GRBs [37]. Figure 5 shows the variations in peak shear displacement and stress with seepage pressure. As the test results indicate, the peak shear displacement of the specimens increases nonlinearly in an upward concave fashion as the seepage pressure increases. Conversely, the peak shear stress decreases nonlinearly in a downward concave manner as the seepage pressure increases. The peak shear stress of the *S*-2, *S*-3, *S*-4, and *S*-5 specimens undergoes reductions of 36.31%, 39.86%, 45.02%, and 50.74% compared to the *S*-1 specimen. This analysis suggests that the softening and erosion effects of seepage water on the specimens intensify with rising seepage pressure, leading to a reduction in the mechanical properties of the specimens. As the seepage pressure increases, the degree of softening in the specimens is enhanced, rendering them more susceptible to deformation.
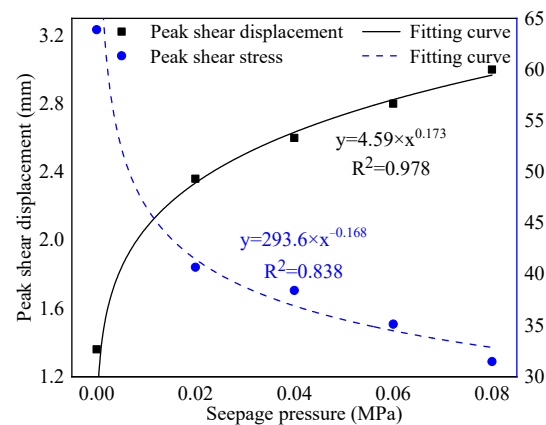
Figure 5. Variations in peak shear displacement and stress with the seepage pressure.

In this study, the seepage velocity and quality can reflect the size of the seepage channel and degree of damage to the GRB under triaxial shear-seepage. The seepage velocity and quality increase with the increase in the seepage pressure, as shown in Figure 6. In order to better understand the change laws of the seepage velocity, waterless (there is no seepage phenomenon), seepage (seepage velocity is less than 2 mL/min), and seepage surge water (seepage velocity is more than 2 mL/min) are defined. Based on the test results, with the increase in the seepage pressure, the seepage behavior changes from waterless ($p \leq 0.02$ MPa, corresponding to specimens *S*-1 and *S*-2) to seepage ($p = 0.04$ MPa, corresponding to specimen *S*-3) and then to seepage surge water ($p \geq 0.06$ MPa, corresponding to specimens *S*-4 and *S*-5).
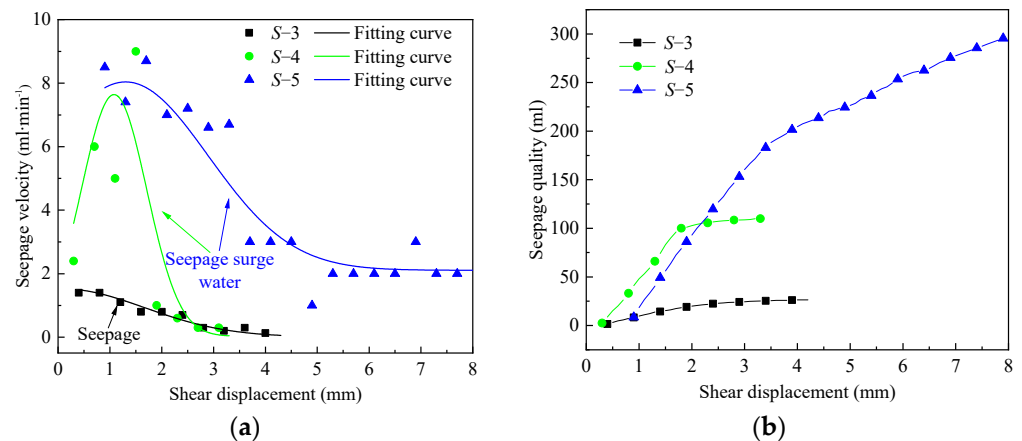

Figure 6. Variations in seepage velocity and quality with the shear displacement of GRB specimens under different seepage pressures. (**a**) Seepage velocity. (**b**) Seepage quality.

Figure 6a shows the variation in seepage velocity with shear displacement. When the seepage pressure is 0.04 MPa (*S*-3 specimen), the seepage velocity (with an initial value of 1.4 mL/min) decreases as the shear displacement increases. When the seepage pressure is 0.06 MPa, the seepage velocity (the initial seepage velocity is 2.4 mL/min) first increases and then decreases with the shear displacement and then reaches a maximum seepage velocity of 8.9 mL/min. When the seepage pressure reaches 0.08 MPa, the seepage velocity (initially 8.5 mL/min) decreases gradually with the increase in shear displacement, and when the shear displacement reaches 5 mm, the seepage velocity stabilizes at 2 mL/min. Therefore, the seepage quality varies greatly under the effect of different seepage pressures, and the seepage qualities are 26.4 mL, 110 mL, and 295.6 mL, respectively (the specimen is *S*-3, *S*-4, and *S*-5 MP, respectively), as shown in Figure 6b. As the seepage pressure becomes higher, the rate of seepage path formation and seepage velocity increase.

4.2. Analysis of Confining Pressure Effects on the Properties of SGRB Specimens

A GRB is usually buried in the ground, and geo-stress has an important influence on its mechanical performance. Different confining pressures were selected to investigate their effects on the seepage characteristic of the GRB under the same seepage pressure and roughness of the soil–slurry interface. The variations in the peak shear displacement and stress with the confining pressure are shown in Figure 7. The test results indicate that the peak shear displacement and stress of the specimens are observably influenced by the confining pressure. The peak shear stress of the specimens increases in a downward, concave, non-linear fashion with the increase in the confining pressure. Correspondingly, the shear displacement decreases with the increase in the confining pressure. With the increase in the confining pressure, the physical and mechanical properties of the specimens are improved.
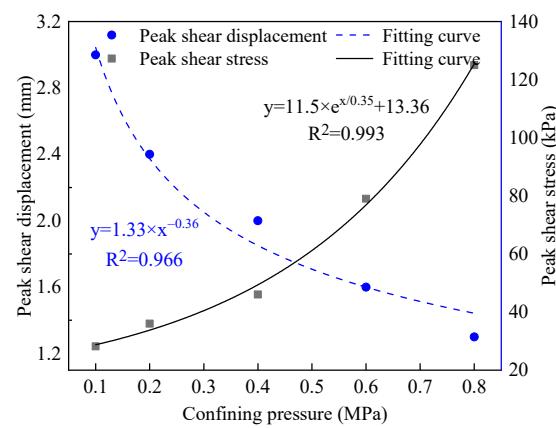

Figure 7. Variations in the peak shear displacement and stress with the confining pressure.

The permeability of the specimens is affected by the confining pressure, leading to reduced permeability in the surrounding rocks as the confining pressure increases. As the test results indicate, at a lower confining pressure ($\sigma_2 \leq 0.2$ MPa), seepage or seepage surge water is observed. Conversely, as the confining pressure increases ($\sigma_2 \geq 0.4$ MPa), no water is observed to flow out from the specimens.

The variations in the seepage velocity and quality with the confining pressure of the *C*-1 and *C*-2 specimens are shown in Figure 8. Figure 8a shows the variation in seepage velocity with shear displacement. Under a confining pressure of 0.1 MPa (*C*-1 specimen), the seepage velocity (initial seepage velocity is 8.5 mL/min) decreases with the increase in the shear displacement, which refers to seepage surge water. With an increased confining pressure of 0.2 MPa (*C*-2 specimen), seepage occurs, characterized by a notably reduced seepage velocity (less than 0.7 mL/min). In addition, the corresponding seepage quality is considerably different, at 309.6 mL (*C*-1 specimen) and 19.9 mL (*C*-2 specimen).

4.3. Analysis of the Soil–Slurry Interface Roughness Effect on the Properties of SGRB Specimens

During seepage failure, a seepage path initially forms at the soil–slurry interface, which is the weak region of the GRB specimens. The seepage characteristics of the specimens are affected by the roughness of the soil–slurry interface. The rough soil–slurry interface can extend the seepage path and thus effectively mitigate the detrimental effects of seepage on the specimens. Figure 9 shows the variation in shear stress with displacement under different roughness levels of the soil–slurry interface in the SGRB. The test results reveal that the shear stress and displacement exhibit a shear softening behavior (*J*-2, *J*-3, and *J*-4 specimens) or sliding behavior (*J*-1 and *J*-5 specimens), depending on the soil–slurry interface roughness. Plastic deformation is less pronounced in the *J*-1 and *J*-5 specimens. Their elastic modulus is comparatively higher than that of the other specimens,

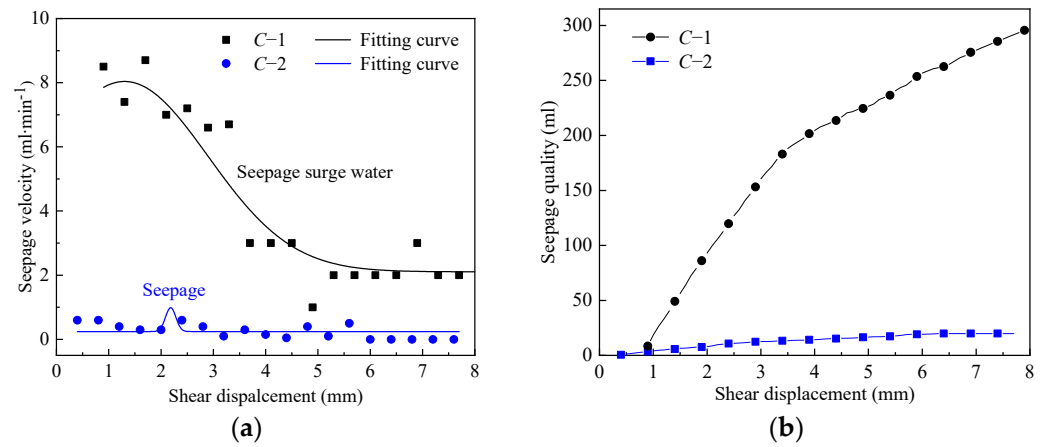exhibiting noticeable plastic deformation, and their residual shear stress demonstrates a decreasing trend.

Figure 8. Variations in the seepage velocity and quality with the confining pressure. (**a**) Seepage velocity. (**b**) Seepage quality.
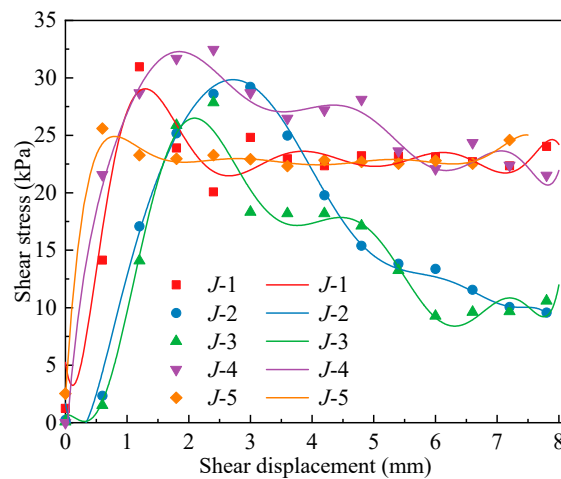

Figure 9. Variation of the shear stress with displacement of the specimens.

The roughness of the soil–slurry interface significantly influences the permeability of the SGRB specimens. The variations in seepage velocity and quality with the roughness of the soil–slurry interface are shown in Figure 10. As the test results indicate, with the increase in the soil–slurry interface roughness coefficient, the seepage velocity first increases and then decreases. Seepage phenomena are observed at the soil–slurry interface when the roughness coefficient is 0~2 (*J*-1 specimen) and 16~18 (*J*-5 specimen), while the other specimens exhibit seepage surge water. This phenomenon can be attributed to the fact that a lower roughness leads to less shear and seepage damage at the soil–slurry interface, resulting in a slower seepage velocity. Conversely, when the roughness of the soil–slurry interface is greater, the slurry vein bulges can obstruct the specimen after shear and seepage damage, resulting in a reduced seepage velocity.
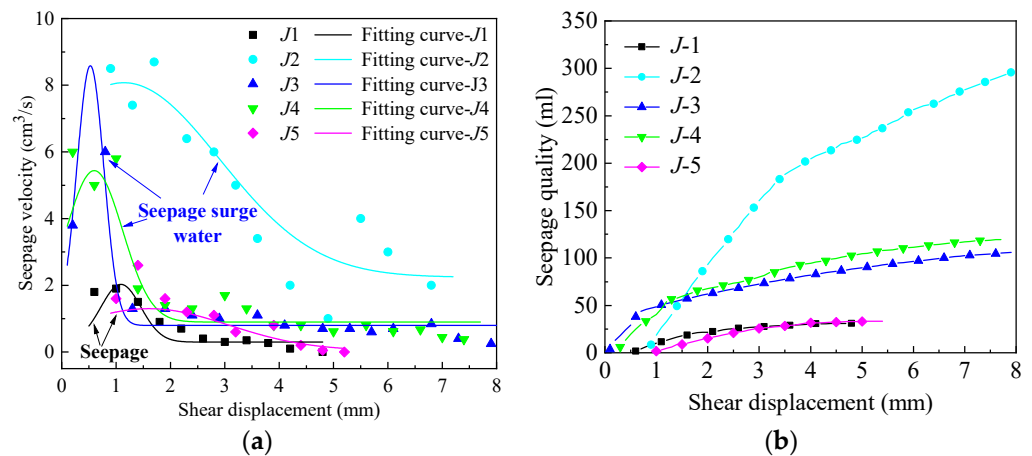
Figure 10. Variations in seepage velocity and quality with the roughness of the soil–slurry interface. (**a**) Seepage velocity. (**b**) Seepage quality.

4.4. Statistical Analysis of the Seepage Performance of SGRB Specimens

The seepage performance statistics of the SGRB specimens are shown in Table 3. The test results demonstrate a significant correlation between the seepage phenomenon and the ratio of seepage pressure to confining pressure, referred to as the 'seepage to confining ratio'. With the increase in the seepage to confining ratio, the seepage quality of the specimen changes from waterless to seepage and then gradually progresses to seepage surge water. A seepage to confining ratio below 0.2 corresponds to a waterless phenomenon. Ratios between 0.4 and 0.6 indicate a seepage phenomenon, and when the ratio is above 0.6, the specimens will exhibit seepage surge water. Based on its correlation with the seepage phenomenon, the 'seepage to confining ratio' is one of the key factors in determining the seepage type in the surrounding rocks. This finding underscores the importance of considering both seepage pressure and confining pressure effects in the design and analysis of GRB structures to ensure their stability and integrity under various loading conditions.

Table 3. Seepage performance statistics of the specimens.

Seepage to Confining Ratio	Seepage Type	Specimen No.
≤0.2	Waterless	*S*-1, 2, *C*-3, 4, 5
0.4–0.6	Seepage	*J*-1, 5, *S*-3, *C*-2
≥0.6	Seepage surge water	*J*-2, 3, 4, *S*-4, 5, *C*-1

4.5. Seepage Failure Mechanism of the GRB

During the tunnel operation period, the soil–slurry interface remains as the weak area within the grouting reinforcement area. Due to significant differences in the physical and mechanical properties of the slurry vein and completely weathered granite, the two materials undergo varying degrees of deformation under the coupling action of geo-stress and groundwater. This incongruous deformation forms a seepage path for groundwater at the soil–slurry interface. When groundwater flows through the seepage path, it continuously washes the slurry veins and completely weathered granite and carries fine particles into the path. Therefore, the seepage velocity of groundwater gradually decreases, and shear-seepage coupling failure occurs after reaching a stable state. When the environment changes, groundwater will continue to erode the soil–slurry interface. While the completely weathered granite undergoes a softening process, groundwater impacts both the cohesion and angle of internal friction of the material. Upon reaching the saturation state, the mechanical properties between the particles of the completely weathered granite weaken further, leading to the potential damage of the GRB due to shear and seepage. Hence, within the framework of geo-stress and groundwater interactions, the GRB undergoes progressive damage, starting with shear and seepage effects before culminating in damage caused by

the seepage water. The described seepage failure mechanism of the SGRB underscores the intricate interplay between geological factors and hydraulic processes after reinforcement.

5. Conclusions and Discussion

The shear-seepage failure behavior of GRBs is a crucial factor affecting the stability of the surrounding rock during tunnel operation. In this study, triaxial shear-seepage tests of SGRB specimens with different slurry vein characteristics were carried out using a modified triaxial shear-seepage coupling test system. The influences of the seepage pressure, confining pressure, and roughness of the soil–slurry interface on the mechanical properties and seepage behavior of the GRB specimens were explored.

The mechanical properties of the SGRBs were reduced under the softening and sub-surface erosion actions of the seepage water, and the peak shear stress of the specimen decreased from 57.25 kPa (waterless) to 29.37 kPa (the seepage pressure was 0.08 MPa), with a reduction of 50.74%. The stability of the surrounding rocks was affected by the water-blocking effect. The shear-seepage process of the GRB showed obvious stages based on the variations in seepage velocity and water turbidity with shear displacement. The seepage phenomenon of the SGRB is related to 'the seepage to confining ratio'. When a seepage disaster occurs in a tunnel during operation, the seepage stage is determined with the seepage velocity, water turbidity, and seepage pressure. This can be used to form a preliminary judgement about the stability of the surrounding rock and provide guidance for control measures.

The roughness of the soil–slurry interface can effectively extend the seepage path, reduce the loss of soil particles, and improve the mechanical properties of the SGRB. Therefore, grouting techniques suitable for water-rich and soft strata that can increase the roughness of slurry veins should be explored further.

However, the shear-seepage process of a SGRB is complicated, and a perfect description of a GRB in engineering conditions is yet to be fully realized. Here, many conditions were simplified, such as the roughness of the soil–slurry interface and pressure loading. Therefore, these simplified factors require further study to improve the seepage failure mechanism.

Author Contributions: Conceptualization, Y.Z. and H.S.; methodology, L.Y.; validation, R.L.; investigation, Y.Z.; resources, L.Y.; data curation, Y.Z.; writing—original draft preparation, Y.Z.; writing—reviewing and editing, H.S. and R.L.; supervision, L.Y. All authors have read and agreed to the published version of the manuscript.

Institutional Review Board Statement: Not applicable.

Informed Consent Statement: Not applicable.

Data Availability Statement: Not applicable.

Conflicts of Interest: The authors declare no conflict of interest.

References

1. Liu, J.; Chen, W.; Yuan, J.; Li, C.; Zhang, Q.; Li, X. Groundwater control and curtain grouting for tunnel construction in completely weathered granite. *Bull. Eng. Geol. Environ.* **2018**, *77*, 515–531. [CrossRef]
2. Li, Z.; Zhang, L.; Sun, D.; Zhang, Q.; Wang, D.; Wang, L. Quantitative design method for grouting in sand layers: Practice in Qingdao metro Line 2. *Processes* **2022**, *10*, 840. [CrossRef]
3. Lu, H.; Yin, J.; Liu, Q.; Cao, A.; Wei, A.; Zhang, K. A self-dissolved grouting reinforcement method for water-rich soft rock roadway. *Bull. Eng. Geol. Environ.* **2022**, *81*, 256. [CrossRef]
4. Wang, X.; Li, R.; Liu, Z.; Jiang, D.; Ji, Z. Comprehensive evaluation of the reinforcement effect of grouting in broken surrounding rock in deep roadways. *Geotech. Geol. Eng.* **2022**, *40*, 2443–2454. [CrossRef]

5. Sha, F.; Li, S.; Lin, C.; Liu, R.; Zhang, Q.; Yang, L.; Li, Z. Research on penetration grouting diffusion experiment and reinforcement mechanism for sandy soil porous media. *Rock Soil Mech.* **2019**, *40*, 4259–4269.

6. Niu, J.; Li, Z.; Gu, W.; Chen, K. Experimental study of split grouting reinforcement mechanism in filling medium and effect evaluation. *Sensors* **2020**, *20*, 3088. [CrossRef]

7. Zhang, L.; Li, Z.; Liu, R.; Zhang, Q.; Li, S. Simulation tests on fracture-compaction grouting process in sand layer. *Chin. J. Geotech. Eng.* **2019**, *41*, 665–675.

8. Meng, L.; Han, L.; Zhu, H.; Dong, W.; Li, W. Study of the effects of compaction and split grouting on the structural strengthening characteristics of weakly cemented argillaceous rock masses. *KSCE J. Civ. Eng.* **2022**, *26*, 1754–1772. [CrossRef]

9. Lan, X.; Zhang, X.; Li, X.; Zhang, J.; Zhou, Z. Experimental study on grouting reinforcement mechanism of heterogeneous fractured rock and soil mass. *Geotech. Geol. Eng.* **2020**, *38*, 4949–4967. [CrossRef]

10. Li, Z.; Li, S.; Liu, H.; Zhang, Q.; Liu, Y. Experimental study on the reinforcement mechanism of segmented split grouting in a soft filling medium. *Processes* **2018**, *6*, 131. [CrossRef]

11. Wang, K.; Li, S.; Yang, L.; Zhang, Q.; Li, Z.; Yuan, J. Grouting simulation experiment on reinforcement characteristics of completely decomposed granite. *Tianjin Univ. Sci. Tech.* **2017**, *50*, 1199–1209.

12. Zhou, X.; Liu, C.; Liu, Y.; Wang, C.; Ma, Y. Effect of dry-wet cycling on the mechanical properties of high-water materials. *Adv. Civ. Eng.* **2020**, *13*, 2605751. [CrossRef]

13. Liu, R.; Li, X.; Liu, Y.; Zhang, Q.; Li, S.; Sun, Z.; Zhang, C. Influence of marine environment on mechanical properties of grout-reinforced body. *Arab. J. Sci. Eng.* **2023**, *48*. [CrossRef]

14. Wen, L.; Luo, Z.; Qin, Y.; Luo, Z. The use of hoek brown failure criterion on determination of the geo-mechanical parameters of a grouting consolidation body. *IEEE Access* **2019**, *7*, 142703–142714. [CrossRef]

15. Deng, C.; Dang, F.; Chen, X.; Miao, Z.; Chen, L. Experimental study on grouting effect and mechanical properties of the rockfill materials grouted with SCM. *Adv. Civ. Eng.* **2020**, *2020*, 8834686. [CrossRef]

16. Liu, L.; Wang, H.; Zheng, S.; Dong, L.; Yu, Y.; Yang, C. Damage model and experimental study of a sand grouting-reinforced body under seepage. *Processes* **2022**, *10*, 256. [CrossRef]

17. Yin, Z.; Zhang, X.; Li, X.; Zhang, J.; Zhang, Q. Modified Burgers model of creep behavior of grouting-reinforced body and its long-term effect on tunnel operation. *Tunn. Undergr. Space Technol.* **2022**, *127*, 104537. [CrossRef]

18. Wang, H.; Liu, Q.; Sun, S.; Zhang, Q.; Li, Z.; Zhang, P. Damage model and experimental study of a sand grouting-reinforced body in a seawater environment. *Water* **2020**, *12*, 2495. [CrossRef]

19. Huang, M.; Xu, C.; Zhan, J.; Wang, J. Comparative study on dynamic properties of argillaceous siltstone and its grouting-reinforced body. *Geomech. Eng.* **2017**, *13*, 333–352.

20. Zang, C.; Yang, L.; Chen, M.; Chen, Y. Study of bearing characteristics and damage law of grouting-reinforced bodies. *Minerals* **2023**, *13*, 591. [CrossRef]

21. Peng, P.; Peng, F.; Sun, Z.; Zhang, D. Property prediction methods of granular soil penetration grouting reinforced body based on fractal theory and Mori-Tanaka method. *Chin. J. Theor. Appl. Mech.* **2022**, *54*, 3099–3112.

22. Huang, Y.; Yang, W.; Zhao, A.; Guo, W. Shear strength and re-failure characteristics of intact red sandstone and grouting-reinforced body of fractured red sandstone under different shear angles. *Minerals* **2023**, *12*, 1580. [CrossRef]

23. Yin, Z.; Zhang, Q.; Zhang, X.; Zhang, J.; Li, X. Shear strength of grouted clay: Comparison of triaxial tests to direct shear tests. *Bull. Eng. Geol. Environ.* **2022**, *81*, 261. [CrossRef]

24. Peng, K.; Zhu, J.; Feng, S.; Wang, R.; Liu, H. An elasto-plastic constitutive model incorporating strain softening and dilatancy for interface thin-layer element and its verification. *J. Cent. South Univ.* **2012**, *19*, 1988–1998. [CrossRef]

25. Zhang, Q.; Zhang, J.; Zhang, T.; Liu, S.; Li, Y.; Xu, G. Experimental analysis and mechanical model of interaction between warm frozen silt and pre-bored grouted planted nodular pile. *Cold Reg. Sci. Technol.* **2022**, *202*, 103632. [CrossRef]

26. Samanta, M.; Punetha, P.; Sharma, M. Influence of surface texture on sand–steel interface strength response. *Geotech. Lett.* **2018**, *8*, 40–48. [CrossRef]

27. Zhao, C.; Zhang, R.; Zhao, C.; Wang, W.; Wang, Y. A three-dimensional evaluation of interface shear behavior between granular material and rough surface. *J. Test. Eval.* **2021**, *49*, 713–727. [CrossRef]

28. Moayed, R.; Hosseinali, M.; Shirkhorshidi, S.; Sheibani, J. Experimental investigation and constitutive modeling of grout-sand interface. *Int. J. Geomech.* **2019**, *19*, 4019024. [CrossRef]

29. Maghool, F.; Arulrajah, A.; Mirzababaei, M.; Suksiripattanapong, C.; Horpibulsuk, S. Interface shear strength properties of geogrid-reinforced steel slags using a large-scale direct shear testing apparatus. *Geotext. Geomembr.* **2020**, *48*, 625–633. [CrossRef]

30. Peng, K.; Zhu, J.; Zhang, D.; Wu, X. Study of mechanical behaviors of interface between coarse-grained soil and concrete by simple shear test. *Chin. J. Rock Mech. Eng.* **2010**, *29*, 1893–1900.

31. Ma, L.; Hu, B.; Chen, Y.; Cui, K.; Ding, J. Shear-seepage properties of intact argillaceous shale under different injection water pressures. *Rock Soil Mech.* **2022**, *43*, 2515–2524.

32. Shi, Z.; Shen, D.; Zhang, Q.; Peng, M.; Li, Q. Experimental study on the coupled shear flow behavior of jointed rock samples. *Eur. J. Environ. Civ. Eng.* **2018**, *22*, 333–350. [CrossRef]

33. Li, Z.; Liu, H.; Dun, Z.; Ren, L.; Fang, J. Grouting effect on rock fracture using shear and seepage assessment. *Constr. Build. Mater.* **2020**, *242*, 118–131. [CrossRef]

34. Zhang, Q.; Li, P.; Zhang, X.; Li, S.; Zhang, W.; Liu, J.; Yu, H. Model test of grouting strengthening mechanism for fault gouge of tunnel. *Chin. J. Rock Mech. Eng.* **2015**, *34*, 924–934.
35. Lee, J.; Han, W.; Kim, S.; Byun, Y. Shear strength and interface friction characteristics of expandable foam grout. *Constr. Build. Mater.* **2020**, *249*, 118719. [CrossRef]
36. Barton, N. Review of a new shear-strength criterion for rock joints. *Eng. Geol.* **1973**, *7*, 287–332. [CrossRef]
37. Wang, H. Study on Penetration, Reinforcement and Deterioration Mechanism of Grouting in Sand Layer under Seawater Erosion-Seepage and Its Application. Ph.D. Thesis, Shandong University, Jinan, China, 2019.